Reflectivity spectra and dielectric function of stage-1 donor intercalation compounds of graphite

J. E. Fischer, J. M. Bloch,* C. C. Shieh,† M. E. Preil,‡ and K. Jelley§
Laboratory for Research on the Structure of Matter, University of Pennsylvania, Philadelphia, Pennsylvania 19104
(Received 13 Noveber 1984)

We have determined the frequency-dependent $\mathscr{E}\perp\mathbf{c}$ dielectric function $\epsilon(\omega)$ for the stage-1 graphite intercalation compounds KC_8, LiC_6, and $KHgC_4$ in the range 0—40 eV, using a combination of normal-incidence reflectivity (0—12 eV) and previously published electron-energy-loss spectra (EELS) (10—40 eV). This provides a better approximation to $\epsilon(q=0,\omega)$ than EELS alone, particularly in the spectral region encompassing the free carrier and π valence plasmons. Successive Kramers-Kronig analyses were performed to obtain the unscreened plasma frequencies for the conduction and π valence electrons and the frequency-dependent effective electron densities $n_{\text{eff}}(\omega)$. For LiC_6 we report 0.5—3.0-eV reflectivity spectra with $\mathscr{E}\|\mathbf{c}$. All three compounds show significant departures from rigid-band behavior, which for LiC_6 is well represented by a band-structure-derived calculation described in the accompanying paper. Intercalant-derived states contribute strongly to the absorption in $KHgC_4$. The free-carrier plasma frequencies and fitted scattering times are in good agreement with the dc conductivities, and the relatively weak optical anisotropy of LiC_6 agrees with theory and therefore can be explained without invoking intercalant-derived or s-like graphitic states at the Fermi energy. Significant shifts in oscillator strength relative to rigid bands are seen in $n_{\text{eff}}(\omega)$, which for all three compounds sums to the correct value at 40 eV.

I. INTRODUCTION

Graphite intercalation compounds exhibit unusual structural and electronic properties, both of which have received considerable attention recently. The prototype stage-1 donor compounds KC_8 and LiC_6 have been extensively studied experimentally and theoretically; detailed band calculations predict the spectra of filled and empty electron states over a wide energy range.[1,2] The metal valence s electron is donated to previously empty graphite π^* orbitals, leaving essentially M^+ ions between the graphite macroanion monolayers. Hybridization between metal and carbon orbitals is weak, leading to departures from a rigid-band picture of 1 eV at most. Two other stage-1 donor compounds have also been studied: BaC_6 and $KHgC_4$. These are more complicated than the alkali-metal binary compounds. In BaC_6 one finds theoretically a significant contribution from Ba-derived d orbitals at the Fermi energy,[3] and the x-ray photoelectron spectrum indicates an unusual internal rearrangement of $6s$ and $5d$ charge around the Ba sites such that only one of the two valence s electrons goes into a conduction band.[4] A number of experiments on the superconducting ternary $KHgC_4$ indicate that the K($4s$) charge is shared between carbon π bands and metal-derived bands,[5,6] in agreement with a symmetry-based model calculation.[6] An *ab initio* band structure for this interesting compound is currently lacking.

A rigorous test of band theory is obtained by calculating the interband dielectric function $\epsilon(q=0,\omega)$ and comparing it with Kramers-Kronig analyzed normal-incidence reflectivity and/or electron-energy-loss spectra (EELS). The experiments reported in this paper were carried out with this goal in mind. A second major goal was to experimentally separate the contributions of conduction and valence electrons in order to accurately determine the corresponding plasma frequencies, in the spirit of the pioneering work by Ehrenreich and Philipp.[7] The simplest realistic optical spectrum of a metal would consist of the free-carrier response, characterized by a plasma frequency ω_p, followed by interband absorption beginning at a threshold $\omega_T \gg \omega_p$. Such a model would give a Drude edge in reflectivity and a free-carrier plasmon peak in $\text{Im}(-1/\epsilon)$ located at ω_p^*, somewhat below ω_p, due to screening by the low-frequency polarizability associated with the interband transitions.[8] Near ω_p^*, the effect of screening in this simple case is to add a constant to ϵ_1 so that information on the free carriers can be extracted from reflectivity or energy-loss data by fitting to a reasonably simple model $\epsilon(\omega)$, i.e., without recourse to Kramers-Kronig analysis. Few if any real metals fall into this category. An unusual situation arises in graphite; two distinct contributions to the interband spectrum approximately satisfy the above criterion.[9] Pure graphite thus provides an excellent model system for quantitative examination of screening effects on interband plasmons since the optical absorption from filled to empty π bands occurs at frequencies well below the corresponding contribution from σ bands. The observed π plasmon loss peak at $\omega_p^*(\pi)=6.3$ eV translates into an unscreened $\omega_p(\pi)$ of 11 eV when the effect of the σ electrons is accounted for.[9] In graphite the free-carrier plasmon is strongly damped by interband $\pi\rightarrow\pi^*$ absorption which extends down to essentially zero frequency ($\omega_T < \omega_p$). Intercalation increases both ω_p and ω_T such that $\omega_T \sim \omega_p$, resulting in observable free-carrier plasmons[10] and Drude edges.[11] However, fitting to model $\epsilon(\omega)$ functions requires a large number of parameters—multiple free-carrier plasmons and/or multiple Lorentz oscillators to represent the interband absorption. Most of the fitting parameters have no counterpart

in band calculations, so this procedure is of limited usefulness for comparing theory and experiment.

We report here the experimental determination of $\epsilon(q=0,\omega)$ for the prototype binary compounds KC_8 and LiC_6, and for a representative ternary compound $KHgC_4$. Results similar to KC_8 were also obtained for RbC_8 and CsC_8. The interesting compound BaC_6 was unfortunately excluded from this study. Most of the results pertain to polarization perpendicular to the c axis, corresponding to near-normal-incidence reflectivity from cleaved surfaces; the Kramers-Kronig analysis requires data over a broad frequency range and is therefore limited to this polarization. The accompanying theoretical paper[12] includes calculations of $\epsilon_{||}(\omega)$ and $\epsilon_{\perp}(\omega)$ for LiC_6. We measured $R_{||}(\omega)$ for LiC_6 at low frequency only, which is, however, sufficient to compare theory and experiment in the free-carrier region for both polarizations.

The present work is complementary to, and draws upon, the energy-loss measurements reported in Refs. 5, 10, and 13. The fundamental quantity of interest is the imaginary component $\epsilon_2(\omega)$, which can be calculated from a band structure and measured via Kramers-Kronig analysis of reflectivity or energy-loss spectra obtained over a wide frequency range. Energy loss has the advantage that it covers an adequate range with one instrument, while reflectivity spectra have better ω resolution and are done at zero momentum transfer. This last difference is especially critical at low frequency; for a strictly free-carrier plasmon, $\epsilon \sim q^2$, and the actual band structure around E_F will be sensitively revealed in the free-carrier dispersion. In both experiments only about 1000 Å of sample is probed along the c direction, corresponding to the optical skin depth in reflectivity or the thickness of the flake in transmission-energy-loss spectroscopy. Kramers-Kronig analyses of energy-loss data over the range 0—40 eV have been published for KC_8,[10] LiC_6,[13] and $KHgC_4$.[5] For KC_8 the derived $R(\omega)$ agrees well with the directly measured spectrum, while for LiC_6 and $KHgC_4$ significant discrepancies occur, especially where R is small, and at low frequency where the Drude contribution dominates. The energy-loss results clearly show the effect of intercalation on the π plasmon, and are indispensable for studying features beyond the high-energy cutoff of the optical equipment: zone-folding features, intercalant-derived transitions, and core levels from carbon and metal atoms. No attempt was made to determine the unscreened plasma frequencies from EELS data alone, nor were the sum rules studied. We feel that the combination of reflectivity and energy-loss data employed previously for graphite[14] and in the present work for the compounds provides the most accurate data for analyzing plasmon screening in the free-carrier and π-valence-electron regions. In particular, extending reflectivity data beyond the high-frequency limit with energy-loss-derived reflectivity should certainly be better than an extrapolation based on pure graphite.

Several studies of the low-frequency optical properties of stage-1 donor compounds have been published. Hennig[15] measured the transmission of thin flakes and was the first to demonstrate Drude-like behavior associated with the metallic character of intercalated graphite. Guerard *et al.*[11] measured normal-incidence reflectivity with the electric vector perpendicular to c for MC_8 (M=K, Rb, Cs), RbC_{24}, RbC_{36}, and BaC_6; since their data extended only to 3 eV, they analyzed the spectra by fitting to a Drude model, and found for stage 1 that two plasmons gave a better fit than a model based on a single group of free carriers. Zanini and Fischer[16] measured stage-1 and -2 K and Cs compounds with || and ⊥ polarization on sputter-etched "a faces." The Drude edge was found to be only slightly anisotropic for stage 1, indicating appreciable three-dimensional (3D) character of the Fermi-surface electron states. LiC_6 was studied by Basu *et al.*[17] and by Pfluger *et al.*;[18] the latter performed a multioscillator fit from 0—6 eV. $KHgC_4$ has been measured by Heinz *et al.*[19] and by Preil and Fischer.[20] The former extrapolated beyond 6 eV with scaled data for graphite to perform a Kramers-Kronig analysis, while the latter used $KHgC_4$ energy-loss data from 6—20 eV and an ω^{-4} extrapolation beyond 20 eV to complete the input data set. Both groups found new structure which had no obvious parentage in the related stage-1 binary compound KC_8, indicating an important contribution from Hg-derived orbitals. Finally, the BaC_6 spectrum of Guerard *et al.*[11] was extended to 6 eV by Preil[21] and Woo,[22] with the remarkable result that the peak around 4 eV associated with graphitic $\pi \rightarrow \pi^*$ transitions is virtually gone. Attempts to obtain vacuum-uv reflectivity and/or energy-loss data to permit detailed study of this effect have been unsuccessful to date.

The paper is organized as follows. In Sec. II we describe the experiments and the strategy employed to assemble data sets as input for Kramers-Kronig analysis. In Sec. III we present the $\mathscr{E} \perp c$ reflectivity spectra and the derived quantities $\epsilon_1(\omega)$ and $\epsilon_2(\omega)$, followed by their decomposition into three plasmon responses: free carriers, π valence electrons, and all valence electrons, respectively, as a function of increasing frequency. The results are discussed in Sec. IV; we begin by comparing with a "diluted graphite" model to clearly display departures from rigid-band effects at high frequency, and then present and discuss the unscreened plasma frequencies and sum rules. For LiC_6 we show the comparison between experiment and theory for both polarizations. The theory is treated in detail in the accompanying paper.[12] Summary and conclusions are found in Sec. V.

II. EXPERIMENTAL DETAILS

In the present study we constructed data sets from four overlapping experiments. Reflectivity data from 0.5 to 11 eV were matched to Kramers-Kronig—derived reflectivity from energy-loss spectra covering the (10—40)-eV range. The absolute R scale is set by measurements from 1.2 to 6.0 eV on an instrument in which a moving detector looks alternately at the incident and reflected beam, thus obviating the need for a reference mirror.[21] A large-area Si photodiode is located as close to the sample as possible to collect most of the nonspecular component from the less-than-perfect sample surfaces. An independent check with a He-Ne laser indicated that the measured reflectivity was underestimated by less than 1% of R due to nonspecularity

ty. The same samples (grown in rectangular Suprasil) were also measured relative to a gold reference mirror from 0.5 to 2.0 eV on another spectrometer. Data from 3.0 to 11.0 eV were obtained from *in situ* cleaved surfaces in a differentially pumped rotating-light-pipe reflectometer attached to a 1-m vacuum monochromator.[23] In this instrument the reflectivity was constant to within 1% for at least 8 h, and the samples were sufficiently thick to permit repeated cleaving. The matching of these three spectra gave constant multiplicative factors in the overlap regions, associated primarily with the reference mirror in the case of the 0.5—2.0 and 1.2—6.0 eV match and with nonspecularity for the 1.2—6.0 and 3.0—11.0 eV overlap. The composite R spectra were then matched to the energy-loss results at 10 eV.

For LiC_6 the low-frequency measurements gave no indication of infrared absorption, so R was smoothly extrapolated via the Drude model to 1.0 at $\omega=0$. This could not be done for KC_8 and $KHgC_4$ since the low-frequency data were clearly not tending toward unity at the lowest frequencies. We attempted to look for discrete ir absorptions without success; the need to transfer the sample into an ampoule with ir windows comprised the surface quality as judged by $R(\omega)$ at higher frequency. Here, the criterion for low-frequency extrapolation was simply to avoid negative ϵ_2 in the analysis. For all three compounds we employed the usual high-frequency extrapolation[8] $R(\omega)=R(\omega')(\omega'/\omega)^s$ in two increments: first, from $\omega'=40$ eV to ω'' with s as a parameter, and then from ω'' to ∞ with $s=4$, the parameters ω'' and s chosen to prevent negative phase shifts. All samples were made from highly oriented pyrolytic graphite using standard techniques; in the case of LiC_6 both vapor- and liquid-phase preparations gave identical results at low frequency, the larger samples obtainable with the liquid method being used for the vacuum-uv experiment.

III. RESULTS

In Fig. 1 we compare the measured reflectivity spectra (solid curves) with spectra derived from energy loss (dashed curves) for KC_8, LiC_6, and $KHgC_4$ in the energy range 0—10 eV in which both experiments were done. For KC_8 the overall agreement is good. In the (4—6)-eV range, energy loss slightly overestimates R, perhaps due to finite q, while the Drude minimum at 2.7 eV and the second minimum near 8 eV are well reproduced. The comparison for LiC_6 is worse; the loss-derived reflectivity is much too high at both minima, and the metallic region 0—2 eV shows spurious structure (part of which may be associated with stage-2 contamination—compare Refs. 17 and 18). For $KHgC_4$ the overall agreement is intermediate to the first two cases, the largest discrepancy occurring between 0 and 2 eV. This figure gives the motivation for using reflectivity plus energy loss to obtain an improved data set for detailed analysis. Thus Fig. 2 shows the composite spectra from 0 to 40 eV, including a spectrum of graphite for comparison. The various regions of response are already evident in the raw data. For graphite and the compounds, R is large at low frequency, due mainly to the free carriers. Unlike graphite, the compounds show Drude-like free-carrier "edges" in the (2—3)-eV region, indicating that ω_T is increased substantially upon intercalation such that the free-carrier plasmon is no longer overdamped by interband transitions.[24] From the Kramers-Kronig analysis described below, ω_p^* is comparable to ω_T for these materials, so the apparent Drude edges are strongly affected by interband

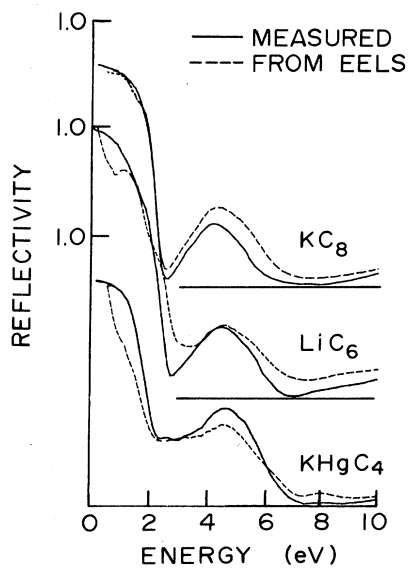

FIG. 1. Comparison of measured normal-incidence reflectivity (solid line) with spectra calculated from Kramers-Kronig—analyzed electron-energy-loss spectra (dashed line), the latter taken from Refs. 10, 13, and 5 for KC_8, LiC_6, and $KHgC_4$, respectively.

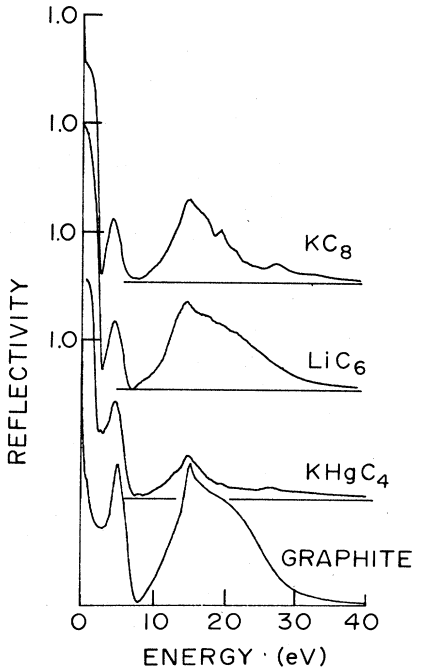

FIG. 2. Reflectivity spectra in the range 0—40 eV obtained by matching the (0—11)-eV direct spectra with EELS results, as described in the text.

absorption, much like the case of silver.[7] The reflectivity peak near 5 eV in all materials is due to $\pi \rightarrow \pi^*$ interband transitions, while the broad structure centered at 15 eV is dominated by the σ bands. Various "fine structures" are also observed; some of this will be discussed later, and the rest has been amply treated in the energy-loss papers.[5,10,13]

Figure 3 shows $\epsilon_1(\omega)$ and $\epsilon_2(\omega)$ resulting from Kramers-Kronig analysis of the composite data in Fig. 2. Insets show more accurately the first zero crossings of $\epsilon_1(\omega)$ which determine the free-carrier plasma frequency screened by interband transitions, denoted ω_p^*(free). These are collected in Table I. In pure graphite the free-carrier resonance is strongly damped by interband transitions, making it extremely difficult to observe. Careful analysis of ir data by Philipp[24] places the unscreened resonance ω_p(free) at 0.44 eV, which is in accord with a theoretical value from Johnson and Dresselhaus.[25] These are included in Table I for comparison. Also included for the compounds are the locations of the corresponding peaks in $\mathrm{Im}(-1/\epsilon)$ observed in the energy-loss spectra measured with minimum q (usually 0.1 Å^{-1}), which should occur close to ω_p^*(free). The agreement is very good. For $KHgC_4$ the free-carrier plasmon peak in energy loss is distorted by interband transitions, so the determination of ω_p^*(free) from the zero crossing of ϵ_1 should be more accurate.

Pure graphite exhibits two zeros in ϵ_1 above the free-carrier region, at 6.8 and 25 eV, identified with plasma resonances of the π and $\pi+\sigma$ valence electrons, respectively.[9] The compounds should exhibit these zeros as well, since energy-loss measurements clearly show two interband plasmon loss peaks. These occur at 5.5 and 20 eV for KC_8 [Fig. 3(a)] and at 6.2 and 25 eV for LiC_6 [Fig. 3(b)]. For $KHgC_4$ [Fig. 3(c)] there is a zero at 6.3 eV with $d\epsilon_1/d\omega > 0$, but the expected third crossing does not occur. We will argue below that this is due to transitions from intercalant-derived levels which screen and damp

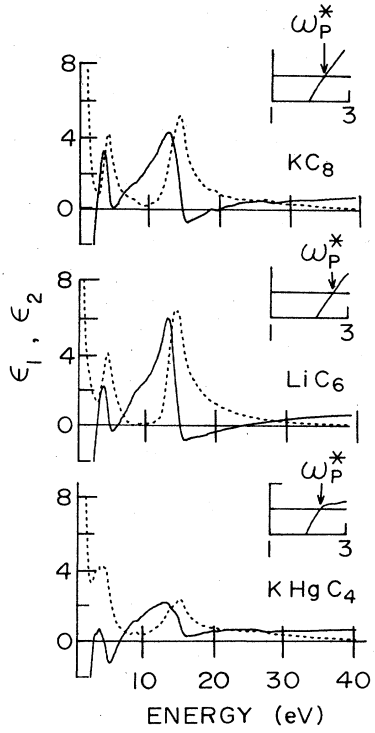

FIG. 3. Kramers-Kronig analyses of the spectra in Fig. 2. Solid line denotes $\epsilon_1(\omega)$; dashed line denotes $\epsilon_2(\omega)$. Insets show the first zero crossings of ϵ_1 in more detail; these correspond to the free-carrier plasma frequencies screened by interband transitions ω_p^*(free); also see Table I.

the $\pi+\sigma$ valence plasmon; the corresponding effect in KC_8 and LiC_6 only occurs at much higher energy. In Table I we list the second zero crossings of ϵ_1 in the column labeled $\omega_p^*(\pi)$, along with the measured positions of the loss peaks. We will discuss later the extent to

TABLE I. Plasma frequencies and interband thresholds with $\mathscr{E} \perp c$. The upper and lower experimental plasma frequencies were obtained from Kramers-Kronig—analyzed reflectivity and peaks in the raw EELS data, respectively.

	ω_p^*(free)		ω_p(free)		E_T		$\omega_p^*(\pi)$		$\omega_p(\pi)$	
	Expt.	Theor.	Expt.	Theor.	Expt.	Theor.	Expt.	Theor.	Expt.	Theor.
KC_8	2.35		4.65	4.5[a]	2.7	2.9[a,b]	5.5		6.0	
	2.38[c]						6.23[c]			
LiC_6	2.65	2.85[d]	5.5	6.8[e]	3.2	2.8[f]	6.2	6.3[d]	7.0	7.5[d]
	2.85[g]					3.3[e]	6.3[g]			
$KHgC_4$	2.33		5.0		1.2, 2.5[h]		6.3		6.85	
	2.2[i]						6.6[i]			
Graphite	0.13[j,k]		0.44[k]	0.5[l]			6.8[m]		11.0[m]	
							7.0[o]			

[a]DiVincenzo, Ref. 1.
[b]Ohno, Ref. 29.
[c]Grunes, Ref. 10.
[d]Chen, Refs. 12 and 32.
[e]Holzwarth, Ref. 33.
[f]Holzwarth, Ref. 2.
[g]Grunes, Ref. 13.
[h]Preil, Ref. 20.
[i]Preil, Ref. 5.
[j]Sato, Ref. 38.
[k]Philipp, Ref. 24.
[l]Johnson, Ref. 25.
[m]Taft, Ref. 9.
[o]Ritsko, Ref. 26.

which these features in the compounds can actually be attributed to transitions involving carbon π states. For KC_8, there is a 0.7-eV discrepancy between values determined by the two methods; smaller discrepancies of the same sense occur for LiC_6 and $KHgC_4$ suggesting that q dispersion is at least partly responsible.

The $\epsilon_2(\omega)$ spectra (dashed curves in Fig. 3) show an initial ω^{-3} dependence from the free carriers, followed by more or less sharp thresholds for interband absorption, which increases with ω to give the peaks near 4 eV. In KC_8 and LiC_6 these peaks are due entirely to $\pi \rightarrow \pi^*$ transitions since there are no occupied intercalant-derived levels that are optically accessible.[1,2] In contrast, $KHgC_4$ shows structure on the 4-eV peak as well as a relatively large value of ϵ_2 at the minimum. Two strategies are possible at this point to clearly separate inter and intraband contributions: one could fit the initial part of $\epsilon_2(\omega)$ with a Drude term and subtract it from the total spectrum to display $\epsilon_2(\text{inter},\omega)$, or one could extrapolate the interband part of $\epsilon_2(\text{total},\omega)$ to lower ω in order to define ω_T. The former is most appropriate in cases where the Drude parameters are constrained, at least in part, by other experimental information, e.g., the Hall coefficient.[7] We choose the latter alternative, using the graphical procedure of Ritsko[26] to obtain ω_T from the leading edge of the 4-eV peak. This defines $\epsilon_2(\text{inter},\omega)$ for the three compounds, with thresholds $\omega_T = 2.7$, 3.2, and 1.3 eV for KC_8, LiC_6, and $KHgC_4$, respectively. These are listed in Table I. We then perform a new Kramers-Kronig integration with $\epsilon_2(\text{inter},\omega)$ as input,

$$\epsilon_1(\text{inter},\omega) = (2/\pi)\int_{\omega_T}^{\infty} \omega'\epsilon_2(\text{inter},\omega')d\omega'/[(\omega')^2-\omega^2] ,$$

and subtract this result from the original data to obtain $\epsilon_1(\text{free},\omega)$, the first zero crossing of which gives the unscreened free-carrier plasma frequency $\omega_p(\text{free})$. The resulting spectra are shown in Fig. 4 with $\omega_p(\text{free})$ listed in Table I. Note that the $\epsilon_1(\text{free},\omega)$ curves extrapolate to unity at high frequency and are structureless, as expected from the Drude form $\epsilon_1(\omega) = 1-\omega_p^2/\omega^2$ (in the limit of infinite scattering time). This indicates that the separation of $\epsilon_2(\text{total})$ into a free-carrier component and an interband component which turns on at ω_T is justified, and that the $\epsilon_1(\text{free},\omega)$ spectrum resulting from the "partial" Kramers-Kronig (KK) integration correctly represents the free carriers. On the other hand, this procedure would not adequately account for weak, localized absorption bands below ω_p since $\epsilon_2(\text{free})$ is so large. Features of this type[27] are observed in higher-stage compounds. We return to the question of low-frequency interband absorption later.

Having removed the free carriers, $\epsilon_1(\text{inter},\omega)$ now clearly shows two well-isolated resonant structures associated with the π and σ interband transitions (dashed curves in Fig. 4). The first zero crossings of $\epsilon_1(\text{inter})$ are essentially

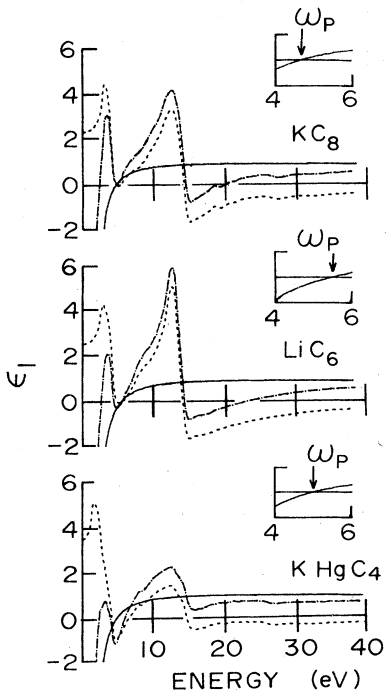

FIG. 4. Decomposition of $\epsilon_1(\omega)$ into free-carrier and interband contributions (see text). Solid line denotes free carriers, dashed line denotes all interband effects, and dotted-dashed line denotes total (i.e., same as solid curves in Fig. 3). Insets show free-carrier contribution in more detail; the zero crossings are the unscreened free-carrier plasma frequencies $\omega_p(\text{free})$; also see Table I.

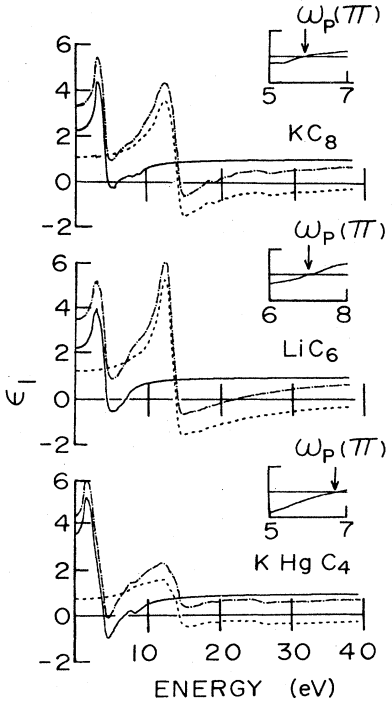

FIG. 5. Decomposition of interband $\epsilon_1(\omega)$ into π and σ contributions, after the method of Ref. 9 (see text). Solid line denotes π contribution, dashed line denotes σ contribution, and dotted-dashed line denotes all interband effects. The latter is the dashed curve of Fig. 4 plus unity, to replace the vacuum contribution to ϵ_1 which was removed with the free-carrier spectrum in the previous decomposition.

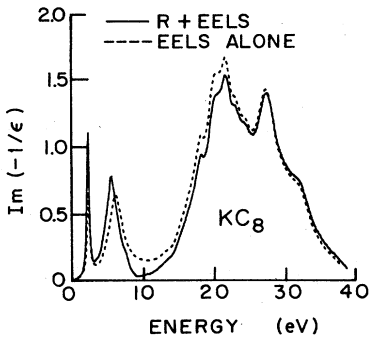

FIG. 6. Comparison of the loss function $\mathrm{Im}(-1/\epsilon)$ for KC_8 as determined from the present data, Fig. 3(a) (solid line), and from EELS (dashed line, Ref. 10).

the $\omega_p^*(\pi)$ previously listed. To find the unscreened values $\omega_p(\pi)$, we use the procedure of Taft and Philipp,[9] based on the occurrence of a second region of transparency near 9 eV [see $\epsilon_2(\omega)$ curves in Fig. 3]. Thus we extrapolate the low-energy side of the 15-eV peak to $\epsilon_2=0$. This occurs at $\omega_T'=9-11$ eV in the compounds, where ω_T' separates the regions of $\pi\rightarrow\pi^*$ and $\sigma\rightarrow\sigma^*$ transitions. The contribution to $\epsilon_1(\omega)$ from the σ transitions alone is then obtained in a manner analogous to the previous separation of free-carrier and interband ($\pi+\sigma$) transitions,

$$\epsilon_1(\sigma,\omega)=(2/\pi)\int_{\omega_T'}^{\infty}\omega'\epsilon_2(\mathrm{inter},\omega')d\omega'/[(\omega')^2-\omega^2]\ ,$$

and subtracting this from $\epsilon_1(\mathrm{inter},\omega)$ (i.e., the curves of Fig. 4) gives $\epsilon_1(\pi,\omega)$, whose zero crossings are the unscreened π plasmon frequencies $\omega_p(\pi)$ listed in Table I. The resulting spectra are shown in Fig. 5.

Finally, we present Fig. 6 as a closure test which compares the measured loss function for KC_8 with the corresponding spectrum calculated from the KK-analyzed data in Fig. 3. The good agreement at high energy indicates that the cumulative error in going from measured $\mathrm{Im}(-1/\epsilon)$ to R and then back to $\mathrm{Im}(-1/\epsilon)$ via ϵ_1 and ϵ_2 is small. The discrepancy near the 10-eV minimum arises from the matching of loss-derived $R(\omega)$ to the smaller values measured directly. Differences in amplitude and position of the free-carrier and π-valence-plasmon losses could be partly due to q dispersion since the loss function was measured with $q=0.1$ Å^{-1}, while the R-derived spectrum corresponds to $q=0$.

IV. DISCUSSION

A. Rigid-band model

One of the first questions one might ask is to what extent is the dielectric function of a compound different from that of graphite? In Fig. 7 we compare the actual $\epsilon_2(\omega)$ spectra (solid curves, from Fig. 3) with the graphite spectrum scaled by the correct carbon atomic density (dashed curves), in order to facilitate overall assessment of the accuracy of a rigid-band approximation. The region above 10 eV is the easiest to interpret. In a rigid-band model it contains only graphitic σ-band contributions; the occupancy of these bands is unchanged by intercalation,

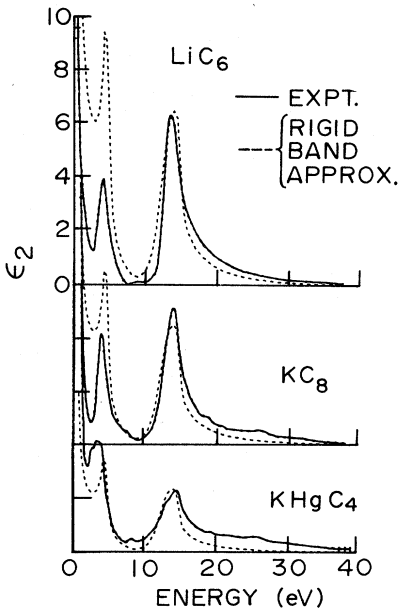

FIG. 7. Comparison of observed $\epsilon_2(\omega)$ from Fig. 3 (solid line), with the graphite spectrum appropriately scaled to account for the decrease in carbon-atom density upon intercalation (dashed line).

and hence the "diluted graphite" $\epsilon_2(\omega)$ should match the actual data very well. For KC_8 [Fig. 7(b)] there is a slight shift of oscillator strength from low to high energy, plus the emergence of fine structure associated with zone folding and potassium core levels.[10] The overall agreement is quite good; the peak amplitude and width are correctly reproduced to within 10%. The same region in LiC_6 [Fig. 7(a)] shows a somewhat greater shift of oscillator strength from below to above the 14-eV peak; the absence of fine structure has been attributed to the MC_6 in-plane zone folding, giving a small joint density of states for new interband transitions;[13] also, the Li($1s$) core level is too deep to be seen, namely 56 eV. The shift in σ oscillator strength is consistent with both band theory[2] and the observation of small nonrigid-band shifts and splittings in angle-resolved photoemission.[28] In contrast to the binary compounds, $KHgC_4$ [Fig. 7(c)] shows substantial absorption in excess of that attributable to graphitic σ transitions. The 15-eV peak amplitude is correctly reproduced, the small value relative to LiC_6 being due to the threefold larger distance between C layers. The peak shape is highly distorted, however, with substantial absorption persisting to very high energy compared to the rigid-band prediction. At 25 eV, for example, the measured ϵ_2 exceeds the simple prediction by a factor of 10. This extra absorption is attributable to the large atomic density of K, and, especially, Hg intercalants in this metal-rich ternary compound, as discussed further below.

The spectral region between 3 and 10 eV is dominated by π-band transitions. For KC_8 and LiC_6 [Figs. 7(b) and 7(a)] the sharply reduced amplitude of the ϵ_2 peak relative to diluted graphite results from the partial filling of the previously empty π^* band, thus reducing the joint density of states for interband transitions. This effect on the π

plasmon has been analyzed quantitatively by Ritsko and Mele[26] and can be understood simply as a modification of the rigid-band model to account for the upward shift of the Fermi energy relative to the (rigid) graphitic bands; in other words, a shift of oscillator strength from the π plasmon to the free-carrier plasmon. In contrast to the binary compounds, Fig. 7(c) again shows more complex behavior for the ternary $KHgC_4$. The oscillator strength in the π-band spectral region is enhanced rather than depleted relative to diluted undoped graphite, particularly just above the interband-transition threshold at 2.4 eV. We have previously identified this extra absorption with new electron states having substantial Hg character.[5,20] The strong departures from graphite-based rigid-band behavior for $KHgC_4$ also show up in the sum rules to be discussed below.

In the lowest-frequency range 0—3 eV, the sharply dropping ϵ_2 for the compounds is dominated by the Drude tail from the free-carrier response, while for diluted graphite the apparently similar drop in ϵ_2 is, in fact, mainly from low-frequency interband transitions. Qualitative comparisons based on the rigid-band model are therefore inappropriate here.

B. Comparison with theory

Going beyond the rigid-band model, we now proceed to compare our optical results with available theory, beginning with KC_8. Recent calculations by Ohno *et al.*[29] and by DiVincenzo and Rabii[1] differ mainly in the location of the K($4s$)-derived band. The former authors place it ~ 2 eV below E_F, whence the charge transfer from K to C is incomplete, while the latter find a minimum 2 eV *above* E_F, indicating complete charge transfer. A calculation of $\epsilon_2(\omega)$ based on the latter model is in progress; in the meantime we can compare our results with predicted interband thresholds, plasma frequencies, and identifiable critical-point transitions.

Both calculations are consistent with our inferred interband $\pi \rightarrow \pi^*$ threshold, 2.7 eV (Table I). It would appear from Ref. 29, however, that partially filled K-derived orbitals produce a large joint density of states between bands of Γ_1^+ and Γ_1^- symmetry at $q=0$, giving additional absorption with a 1-eV threshold. We do not observe such a threshold, nor any significant interband damping of the screened free-carrier plasmon at 2.35 eV. DiVincenzo predicts instead weak interband transitions at very low energy, which may explain why the reflectivity is only 80% at 0.5 eV (Fig. 1). As noted earlier, attempts to extend the measurements below 0.5 eV have been unsuccessful. DiVincenzo calculated ω_p(free) for both polarizations; his value of 4.65 eV for $\mathscr{E} \perp \mathbf{c}$ agrees well with the experimental value, 4.5 eV (Table I). Ohno *et al.* did not calculate ω_p(free), but we can assume that it would exceed the experimental value substantially due to the additional partially filled band. Indeed, Ohno's $N(E_F)$ exceeds the experimental value from spin susceptibility[30] by a factor of 2, while DiVincenzo's is in good agreement. On the other hand, DiVincenzo's ω_p(free) value with $\mathscr{E} \| \mathbf{c}$ is only 0.3 eV, much lower than the experimental screened ω_p^*(free) value of 1.6 eV, obtained from polarized measurements on sputter-etched "*a* faces."[17] The relatively weak experimental anisotropy of the free-carrier optical response is inconsistent with a Fermi surface made up entirely of 2D π-like electron states. On this basis, Ohno's band structure would be more compatible with experiment, although definite conclusions must await a calculation of ϵ_2 for both polarizations. Finally, we point out the weak feature in $\epsilon_2(\omega)$ for KC_8 at 7.6 eV (Fig. 3), which can be identified with an interband critical point at 8.5 eV in both calculations. We conclude that for KC_8 there is, on balance, nothing in the optical data which definitely favors one band calculation or the other, although the recent valence-band x-ray-photoelectron—spectroscopy[31] (XPS) and absolute-spin-susceptibility[30] results are inconsistent with a significant contribution of *s*-like states.

The theoretical situation for LiC_6 is further advanced, as described in Ref. 32 and the accompanying paper.[12] Briefly, Chen *et al.* calculated ϵ(total, ω) by combining the theoretical plasma tensor of Holzwarth *et al.*[33] as a Drude term with an interband spectrum (including matrix elements) derived from a new self-consistent mixed-basis pseudopotential band structure.[2] Figure 8 compares theory and experiment for ϵ_1 and ϵ_2 with $\mathscr{E} \perp \mathbf{c}$; the overall agreement is seen to be excellent. The screened free-carrier plasma frequency ω_p^*(free) is predicted to occur at 2.9 eV, determined by the zero crossing of $\epsilon_1(\omega)$. Holzwarth originally found ω_p(free) = 6.8 eV, so the interband screening effect is very strong for this polarization. The measured ω_p^*(free) is 2.65 eV, in remarkably good agreement considering that the theoretical quantity is defined by the entire interband spectrum as well as by the Fermi-surface properties. The $\pi \rightarrow \pi^*$ absorption which dominates ϵ_2 in the range 3—7 eV is accurately reproduced. The unscreened π plasmon is predicted to occur at

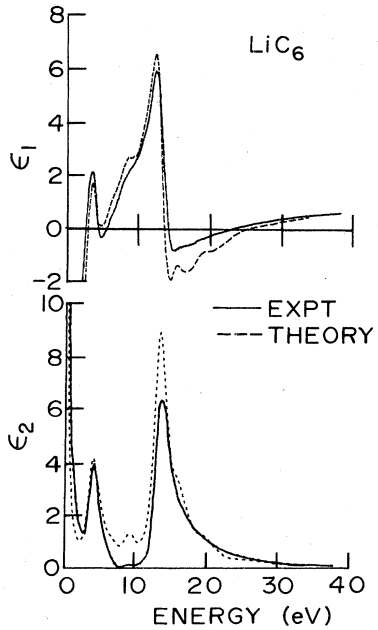

FIG. 8. Comparison of experimental (solid line) and theoretical (dashed line, Refs. 12 and 32) $\epsilon_1(\omega)$ and $\epsilon_2(\omega)$ with $\mathscr{E} \perp \mathbf{c}$ for LiC_6.

7.5 eV, in good agreement with the experimental value of 7.0 eV. The most pronounced discrepancy occurs in the transparent region between 7 and 11 eV, where theory overestimates ϵ_2 substantially. Nonetheless, two interband critical points are correctly predicted to within 0.4 eV. These transitions can be attributed to the folding of the graphite K point back to the zone center by the $\sqrt{3}\times\sqrt{3}$ superlattice. They occur at 8.4 and 9.1 eV in our experiment, compared to 8.8 and 9.4 eV in the theory. These weak transitions were not observed in the energy-loss spectra, probably because the finite q permits nonvertical transitions which smear the spectrum to obscure weak vertical transitions. Finally, theory predicts structure in ϵ_2 at 16 and 20 eV associated with additional critical points induced by zone folding. Experiment is limited to EELS in this spectral range; no structure is observed, probably because the weak zone-folding effects[13] are obscured by noncritical transitions and finite-q effects. Comparing Figs. 7(a) and 8(b) we see that the full $\epsilon_2(\omega)$ calculation correctly reproduces the gross shift of absorption from below to above the ϵ_2 peak at 14 eV, a notable failure of the rigid-band model.

Chen also calculated[32] $\epsilon(\text{total},\omega)$ for $\mathscr{E}||\mathbf{c}$. Measurements in this configuration are limited by the poor quality of reflecting surfaces containing the **c** axis.[16] We measured $R_{||}(\omega)$ for LiC_6 in the range 0.5—0.3 eV, clearly insufficient for KK analysis. Instead, $R_{||}(\omega)$ was calculated from the theoretical interband dielectric function[32] and plasma tensor;[33] the comparison between theory and experiment is shown in Fig. 9. Both theory and experiment show metallic behavior, albeit with lower ω_p^*(free) than for $\mathscr{E}\perp\mathbf{c}$. The band structures on which the calculation is based have only graphitic π states at the Fermi surface, so the metallic behavior with $\mathscr{E}||\mathbf{c}$ must result from **c**-axis dispersion of these states rather than from a 3D intercalant-derived contribution to $N(E_F)$. This is not unexpected for LiC_6; the C layers are only expanded 10% relative to graphite, the A-A stacking actually enhances the overall near-neighbor overlap between C atoms on adjacent layers, and the graphite π bands become more three dimensional as the Fermi energy increases above the K-point degeneracy. Lacking an accurate and complete data set for $\mathscr{E}||\mathbf{c}$, we cannot obtain ω_p directly from Kramers-Kronig analysis and breakdown into free and interband terms. However, we can approximate ω_p^* as the midpoint of the Drude edge in $R(\omega)$, from which we find 1.2 and 1.5 eV from theory and experiment, respectively. This is again remarkably good agreement, the combined theoretical inputs correctly accounting for interband screening of the $\mathscr{E}||\mathbf{c}$ plasmon from 2.2 eV to near its observed value. We conclude that for LiC_6 the measured $\epsilon(\omega)$ agrees very well with theory, with respect to both interband transitions and free-carrier plasmon anisotropy. In particular, small but significant deviations from rigid-band behavior show up in the data and are well explained by the theory, and the 3D character of the Fermi surface is attributable to **c**-axis dispersion of graphite-derived π bands rather than from a partly filled s-like[34] or intercalant-derived band.

Finally, we consider $KHgC_4$. Lacking theoretical guidance, it would appear sensible to compare its properties

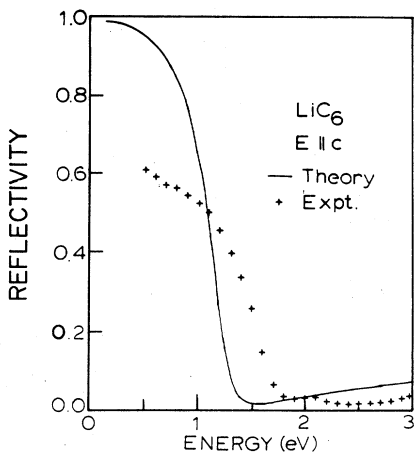

FIG. 9. Reflectivity spectra for LiC_6 with $\mathscr{E}||\mathbf{c}$—experiment (pluses) and theory (solid line, Ref. 12).

with those of the related binary compound KC_8. Several differences have already been noted earlier.

Figure 4(c) shows the decomposition of ϵ_2 into free-carrier and interband contributions, the inset giving $\omega_p(\text{free})=5.0$ eV, only slightly higher than the value of 4.65 eV for KC_8, see Table I. This could be quite simply explained by assuming that all the K($4s$) charge is transferred to graphite π bands in both compounds, the higher K-atom density in $KHgC_4$ being offset by the lower C-atom density relative to KC_8. There is ample evidence, however, that the transferred charge per C atom, not per volume, is indeed the same: The $\pi\rightarrow\pi^*$ interband thresholds,[20] the π-plasmon oscillator strengths,[5] and the C($1s$) binding energies[20] are totally inconsistent with substantially greater π charge per C atom in $KHgC_4$ relative to KC_8. Thus the nearly equal, unscreened free-carrier plasma frequencies are most likely fortuitous, reflecting the balance among the densities and masses of different carrier types in the two compounds.

A notable difference between KC_8 and $KHgC_4$ is the existence in the latter of anomalously strong absorption in the region of the interband threshold. This can be seen by comparing Figs. 3(a) and 3(c), and referring to the rigid-band analysis in Fig. 7. The extra structure in the 4-eV peak in ϵ_2 has previously been identified with an interband threshold of 1.3 eV between intercalant-derived bands which lies below the 2.5 eV $\pi\rightarrow\pi^*$ threshold.[20] Careful examination of the ϵ_2 spectrum in Fig. 3 reveals weak structure at about 8 and 11 eV which might be associated with transitions originating from the Hg($5d$) doublet. X-ray-photoelectron spectroscopy of Hg metal gives 7.6 and 9.8 eV for the $5d$ binding energies relative to E_F; similar XPS peaks are found in $KHgC_4$.[20] If this assignment is correct, then the empty states having appreciable spatial overlap with the Hg($5d$) core orbitals have a threshold 0.5—1.0 eV above E_F.

Dramatic differences between KC_8 and $KHgC_4$ are found above the region of the π-band absorptions, as pointed out in Figs. 7(b) and 7(c) vis-à-vis rigid bands. These will be discussed below in the context of the sum rules.

C. Plasmons and screening

The decomposition procedure described in Sec. III should produce $\epsilon_1(\text{free},\omega)$ spectra which are purely Drude in spectral character, as noted earlier. Since the procedure uniquely defines the $\omega_p(\text{free})$ values listed in Table I, one should be able to fit the $\epsilon_1(\text{free},\omega)$ spectra in Fig. 4 with a Drude model in which the scattering time τ is the only adjustable parameter. For all three compounds a satisfactory fit is obtained with $\tau=2\times10^{-14}$ sec, which can be combined with $\omega_p(\text{free})$ from Table I to estimate the conductivity $\sigma=\tau\omega_p^2(\text{free})/4\pi$. The resulting values are in the range $(1.1-1.5)\times10^5\ \Omega^{-1}\,\text{cm}^{-1}$, in good agreement with the directly measured quantities.[11,17] Previous attempts to reconcile the optical and dc conductivity were based on model fits to $R(\omega)$ including Lorentz oscillators, multiple carrier groups, or *ad hoc* complex background dielectric constants to account for interband screening.[11] The present results with only one free parameter are gratifying. From Table I we see that all three compounds exhibit similar screening shifts of the free-carrier plasma frequency, indicating the overall similarity of their interband absorption spectra.

We turn now to the π valence plasmon $\omega_p(\pi)$. Table I shows that intercalation reduces $\omega_p(\pi)$ relative to pure graphite, an effect which is dominated by the transfer of intercalant valence electrons to previously empty π states. Quantitative comparison with a rigid-band model can be done via a partial sum rule $\int\omega\epsilon_2 d\omega$, the integral spanning the first interband peak in ϵ_2, Fig. 3. This integral for the compounds should scale, with respect to its graphite value, with the layer spacing, a large effect, and the π charge per C atom, a small one even assuming complete ionization. This rigid-band scaling is obeyed by KC_8 and KC_{24} but not by $KHgC_4$,[5,20] as is also evident from Fig. 7. The presence of additional interband absorption in the ternary compound is clear and also accounts for the nonmonotonic trend in $\omega_p(\pi)$ with layer separation, viz., 11.0, 7.9, 6.0, and 6.85 eV as the C layer spacing increases from 3.35 to 3.7 to 5.4 to 10.2 Å. The $KHgC_4$ value is anomalously high because the effective number of electrons in this frequency range includes a significant contribution from Hg.

From Table I we see in all cases that the screening effect of transitions above $\omega_p(\pi)$ is much less in the compounds than in pure graphite; $\omega_p^*(\pi)$ is only 0.5—0.8 eV below $\omega_p(\pi)$ compared to the 4-eV shift in graphite.[9] This is rather curious and may be coincidental; for graphite, LiC_6 and KC_8 this screening is certainly dominated by $\sigma\rightarrow\sigma^*$ transitions which should be identical. We have no simple physical argument for why this is so. Nonetheless, $\tilde{\epsilon}(\omega)$ calculations for graphite (Ref. 35) and LiC_6 (Refs. 12 and 32), correctly reproduce these differences in the effects of σ transitions on the π plasmon.

D. Sum rules

Figure 10 compares the frequency-dependent effective electron-density sum rule

$$n_{\text{eff}}(\omega)=\frac{m}{2\pi^2e^2}\int_0^{\omega}\omega'\epsilon_2(\omega')d\omega'$$

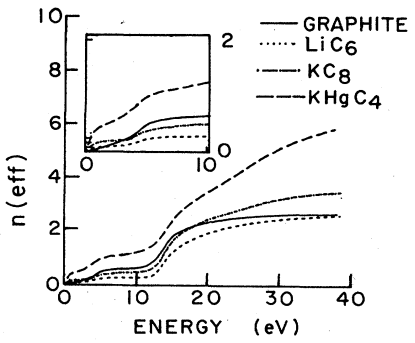

FIG. 10. $n_{\text{eff}}(\omega)$ for graphite (solid line), LiC_6 (short-dashed line), KC_8 (dotted-dashed line), and $KHgC_4$ (long-dashed line)—also see Table II.

for graphite and the intercalation compounds (normalized per C atom). For graphite, the spectral separation between $\pi\rightarrow\pi^*$ and $\sigma\rightarrow\sigma^*$ transitions with $\mathscr{E}\perp c$ should lead to two plateaus in $n_{\text{eff}}(\omega)$ at 1 and 4 e/atom, as was indeed found by Taft and Philipp.[9] We were unable to reproduce these plateau values exactly; our data and analysis gave instead 0.6 and 2.7 e/atom (solid curve in Fig. 10). The first plateau corresponds to the transparent region centered at 9 eV which separates the π and σ absorption, while the second plateau extends from 25 eV to the upper limit of the experiment. The overall shape is similar to that obtained by Taft and Philipp, so we can account for the quantitative difference by a correction factor. We assume that the same factor applies to the n_{eff} curves for the compounds and justify the assumption later. With this caveat we can proceed to compare the $n_{\text{eff}}(\omega)$ spectra of the compounds with our graphite results.

Referring first to the inset, we see qualitatively different initial behavior for $n_{\text{eff}}(\omega)$, graphite showing a gradual increase due to a quasicontinuous spectrum of interband transitions beginning at $\omega=0$, while the compounds show the steplike behavior characteristic of the Drude response of the free electrons. The first plateaus for the compounds should give the free-electron fraction per C atom; we take the value $n_{\text{eff}}(2\text{ eV})$ as an approximate measure since $KHgC_4$ really has no first plateau. Scaling by the aforementioned error in the corresponding graphite curve, we find 0.18, 0.36, and 0.63 e/C atom for LiC_6, KC_8, and $KHgC_4$, respectively (Table II). The LiC_6 value is nicely accounted for by the $\frac{1}{6}$ e/C atom transferred from Li which is now Li^+, and the absence of interband

TABLE II. $n_{\text{eff}}(\omega)$ in e/C atom, evaluated from zero to 2, 9, and 38 eV; comparison is made with the electron count for atomic transitions up to 40 eV (see text).

ω	KC_8	LiC	$KHgC_4$	Graphite
2 eV	0.36	0.18	0.63	0.08
9 eV	0.81	0.44	1.90	1.0
38 eV	5.20	3.90	8.76	4.0
Electron count (to 40 eV)	5.12	4.17	9.25	4.0

absorption below 3.2 eV (indicated most sensitively by the fact that $R \rightarrow 1$ as $\omega \rightarrow 0$, Fig. 1). If KC_8 behaved similarly, one would expect 0.12 e/C atom at 2 eV, assuming complete charge transfer; the extra 0.24 e/C atom actually observed represents the low-frequency interband absorption below the $\pi \rightarrow \pi^*$ threshold which causes the reflectivity to asymptotically tend to a value of ~ 0.8 at low frequency (Fig. 1). The anomalously large value 0.63 for $KHgC_4$ reflects the additional interband threshold at 1.2 eV which has been tentatively attributed to bands involving Hg orbitals.

The three compounds differ markedly in their behavior vis-à-vis graphite at the second plateau (inset of Fig. 10). Taking 9 eV as the energy where intraband- and interband π transitions should be exhausted, we find in Table II that the KC_8 value (relative to graphite) is slightly below the expected value of 1.12 [1 C(π) plus $\frac{1}{8}$ K($4s$)], while for LiC_6 the corrected value is less than half of what one expects from a rigid-band interpretation. In contrast, n_{eff}(9 eV) for $KHgC_4$ exceeds a rigid-band prediction by almost a factor of 2. The small discrepancy for KC_8 probably results in part from the inaccuracy in our determination of n_{eff}, since the partial sum rule for the $\pi \rightarrow \pi^*$ peak in ϵ_2 does in fact scale properly with graphite, indicating that there is indeed approximately 1 π electron per C atom contributing to the absorption in this region.[5] For LiC_6, on the other hand, both the energy-loss and reflectivity experiments show that the $\pi \rightarrow \pi^*$ peak in ϵ_2 has a magnitude ~ 4 [Fig. 3(b)] compared to 10 for graphite, which results in the anomalously small value for n_{eff}(9 eV). The implication is that some of the oscillator strength is shifted to higher energy, as we will argue in a moment. We point out that the theoretical magnitude of $\epsilon_2(\omega)$ is in good agreement with experiment [Fig. 8(b)], and so, regardless of the reason for the sharply reduced n_{eff} relative to graphite, it is correctly reproduced by the band-structure calculation. Finally, the corresponding value for $KHgC_4$ is found to be 1.90, whereas the largest one could possibly expect on a rigid-band basis (i.e., ignoring Hg) would be 1.25 if all the K($4s$) charge were to go into the π states, a hypothesis which we have already disproved. The anomalously large n_{eff}(9 eV) clearly indicates extensive interband contributions from states with intercalant-derived character, no doubt involving Hg orbitals.

Referring finally to the overall curves in Fig. 10, we first point out that the sum rule for LiC_6 eventually reaches a value close to that of graphite, indicating that our scaling correction is accurate to about 0.3 e/C atom, or 10%. As expected, there is no discernible structure to signal the onset of contributions from deep valence or core states, while n_{eff} saturates more slowly than for graphite. In Table II we compare the corrected n_{eff}(38 eV) with the expected number of electrons, which for LiC_6 is quite satisfactory. This gives us confidence in the interpretation of the small n_{eff}(9 eV) as indicating a substantial shift of oscillator strength from the π to the σ region of interband energy, which could result, for example, from π-σ hybridization in either the valence or conduction bands.[2,33] We point out that nonrigid shifts of order 1 eV have been detected experimentally for both the filled[28] and empty[36] states of LiC_6. Turning to KC_8, the overall curve shows a weak change in slope at 23 eV which is probably associated with transitions involving K($3p$) initial states. We see a reasonably saturated n_{eff} at 38 eV equal to 5.2 e/C atom after correction, to be compared to 5.12 if we add the K($3p$) and K($3s$) electrons to the count; the relevant binding energies are ~ 18 and ~ 35 eV, respectively. Structure associated with the $3p$ levels (0.75 e/C atom) is in fact observed in ϵ_2 at 18 eV [Fig. 3(a)], while we do not see directly the $3s$ level (0.25 e/C atom). This could be interpreted as evidence for an appreciable density of empty states with s character, e.g., the K($4s$) or interlayer band,[34] consistent with DiVincenzo's calculation.[1] If one deconvolves a free-electron band into angular-momentum components, the s-like character is large near the band minimum, while the p-like contribution has its greatest amplitude somewhat above the band minimum. Thus an empty free-electron-like band would have s character at threshold, so the matrix element for dipole transitions from s-like initial states would be small.

The $n_{\text{eff}}(\omega)$ curve for $KHgC_4$ also shows a slope change at 23 eV which could be associated with K($3p$) levels; see also Fig. 3(c). In contrast to graphite, LiC_6, and KC_8, n_{eff} is still increasing with ω at 38 eV. The corrected value 8.76 nonetheless agrees well with the electron count 9.25, in which we include the Hg($6s$) and Hg($5d$) levels contributing 0.5 and 2.5 e/C atom, respectively.

The sum-rule analysis thus confirms the existence of significant nonrigid-band effects within the π and σ manifolds of the simple binary compound LiC_6 (and possibly also KC_8, albeit to a lesser degree), as well as the strong contribution from Hg-derived states to the dielectric response of $KHgC_4$. This trend is consistent with what one would expect based on the small but significant changes in the in-plane C—C bond lengths of the compounds relative to graphite. Pietronero and Strassler first pointed out the linear relation between σ bond-length expansion and excess π charge per C atom.[37] On this basis, LiC_6 exhibits the largest dilation of the σ bond resulting from an increase in the π charge, consistent with the relatively large nonrigid-band effects manifested by $\epsilon_2(\omega)$ and $n_{\text{eff}}(\omega)$.

V. SUMMARY

We have performed Kramers-Kronig analyses of combined reflectivity and energy-loss data to obtain $\epsilon_1(\omega)$ and $\epsilon_2(\omega)$ spectra for the prototype compounds KC_8, LiC_6, and $KHgC_4$. Two decompositions of ϵ_2(total) yield accurate values of the unscreened plasma frequencies for free electrons and for π valence electrons. The deduced free-carrier parameters agree well with measured conductivities without invoking multiple carrier groups. Significant departures from rigid-band behavior are manifested by a shift in oscillator strength from π to σ features (LiC_6), and from new absorption clearly associated with intercalant-derived states ($KHgC_4$). The positions and oscillator strengths of the π-band features reflect the net effect of charge transfer, carbon-sublattice dilation, intercalant-derived levels, and π-σ hybridization in the various compounds. For the single case of LiC_6, theory and experiment are in good agreement for both polarizations, confirming the accuracy of the *ab initio* band-

structure strategies developed by our colleagues at the University of Pennsylvania, and demonstrating that substantial 3D coupling occurs without participation of intercalant-derived s bands or s-like graphitic (interlayer) bands. Much new structure is seen in $KHgC_4$ relative to KC_8; it would be extremely interesting to study these in detail with the appropriate angle-resolved electron spectroscopies. We also await a calculation of ϵ_2 for KC_8 to assess the validity of our more speculative interpretations.

ACKNOWLEDGMENTS

We have benefited greatly from the ongoing collaboration with Professor S. Rabii's theory group, in particular N.-X. Chen and R. C. Tatar. Dr. H. Philipp graciously provided a listing of his graphite data and analysis which helped enormously in the initial phases. Thanks are also due Dr. A. Moore of Union Carbide for donating the highly oriented pyrolytic graphite. Helen Mertwoy prepared some of the samples, and Dr. R. L. Schmidt participated in the early work. Financial support from the U.S. Army Research Office (ARO) under Contract No. DAAG-29-80K-0019 and from the National Science Foundation Materials Research Laboratories (NSF-MRL) Program under Grant No. DMR-82-16718 is gratefully acknowledged.

*Present address: Department of Physics, Brookhaven National Laboratory, Bldg. 510E, Upton, NY 11973.
†Present address: AT&T Bell Laboratories, Holmdel, NJ 07733.
‡Present address: Advanced Micro Devices, P. O. Box 3453, Sunnyvale, CA 94088.
§Present address: Department of Electrical Engineering, University of Illinois at Chicago, Chicago, IL 60680.

[1]D. P. DiVincenzo and S. Rabii, Phys. Rev. B **25**, 4110 (1982).
[2]N. A. W. Holzwarth, S. G. Louie, and S. Rabii, Phys. Rev. B **28**, 1013 (1983).
[3]N. A. W. Holzwarth, D. P. DiVincenzo, R. C. Tatar, and S. Rabii, Int. J. Quantum Chem. **23**, 1223 (1983).
[4]M. E. Preil, J. E. Fischer, S. B. DiCenzo, and G. K. Wertheim, Phys. Rev. B **30**, 3536 (1984).
[5]M. E. Preil, L. A. Grunes, J. J. Ritsko, and J. E. Fischer, Phys. Rev. B **30**, 5852 (1984).
[6]G. Timp, P. D. Dresselhaus, and G. Dreselhaus, Bull. Am. Phys. Soc. **29**, 295 (1984).
[7]H. Ehrenreich and H. R. Philipp, Phys. Rev. **128**, 1622 (1962).
[8]F. Wooten, *Optical Properties of Solids* (Academic, New York, 1972).
[9]E. A. Taft and H. R. Philipp, Phys. Rev. **138**, A197 (1965).
[10]L. A. Grunes and J. J. Ritsko, Phys. Rev. B **28**, 3439 (1983).
[11]D. Guerard, G. M. T. Foley, M. Zanini, and J. E. Fischer, Nuovo Cimento **38B**, 410 (1977).
[12]N.-X. Chen and S. Rabii, following paper [Phys. Rev. B **31**, 4784 (1985)].
[13]L. A. Grunes, I. P. Gates, J. J. Ritsko, E. J. Mele, D. P. DiVincenzo, M. E. Preil, and J. E. Fischer, Phys. Rev. B **28**, 6681 (1983).
[14]E. Tosatti and F. Bassani, Il Nuovo Cimento **65B**, 161 (1970).
[15]G. R. Hennig, J. Chem. Phys. **43**, 1201 (1965).
[16]M. Zanini and J. E. Fischer, Mater. Sci. Eng. **31**, 169 (1977).
[17]S. Basu, C. Zeller, P. J. Flanders, C. D. Fuerst, W. D. Johnson, and J. E. Fischer, Mater. Sci. Eng. **38**, 275 (1979).
[18]P. Pfluger, E. Schupfer, R. Lapka, and H. J. Güntherodt, in *Extended Abstracts of 15th Biennial Conference on Carbon*, edited by W. C. Forsman (American Carbon Society, University Park, PA, 1981), p. 70.
[19]R. E. Heinz and P. C. Eklund, in *Intercalated Graphite*, edited by M. S. Dresselhaus, J. E. Fischer, and M. I. Moran (North-Holland, New York, 1983), p. 81.
[20]M. E. Preil and J. E. Fischer, Synth. Met. **8**, 149 (1983).
[21]M. E. Preil, Ph.D. thesis, University of Pennsylvania, 1983.
[22]K. C. Woo, P. J. Flanders, and J. E. Fischer, Bull. Am. Phys. Soc. **27**, 272 (1982).
[23]Similar in design to the instrument described by G. W. Rubloff [Appl. Opt. **8**, 305 (1969)]. Incident and reflected intensities were collected sequentially by the light pipe and divided separately for each rotation by an analog divider, the resulting values being averaged over many rotations to obtain a desired signal-to-noise ratio. We found this method to be more accurate than the conventional boxcar approach in which the incident and reflected signals are averaged separately and then divided to yield the reflectivity value.
[24]H. R. Philipp, Phys. Rev. B **16**, 2896 (1977).
[25]L. G. Johnson and G. Dresselhaus, Phys. Rev. B **7**, 2275 (1973).
[26]J. J. Ritsko and E. J. Mele, Phys. Rev. B **21**, 730 (1980).
[27]R. E. Heinz, G. Doll, P. Charron, and P. C. Eklund, in *Intercalated Graphite*, Ref. 19, p. 87.
[28]W. Eberhardt, I. McGovern, E. W. Plummer, and J. E. Fischer, Phys. Rev. Lett. **44**, 200 (1980).
[29]T. Ohno, K. Nakao, and H. Kamimura, J. Phys. Soc. Jpn. **47**, 1125 (1979).
[30]S. Ikehata, H. Suematsu, and S. Tanuma, Solid State Commun. **50**, 375 (1984).
[31]M. E. Preil and J. E. Fischer, Phys. Rev. Lett. **52**, 1141 (1984).
[32]N.-X. Chen and S. Rabii, Phys. Rev. Lett. **52**, 2386 (1984).
[33]N. A. W. Holzwarth, S. Rabii, and L. A. Girifalco, Phys. Rev. B **18**, 5190 (1978).
[34]M. Posternak, A. Baldereschi, A. J. Freeman, E. Wimmer, and M. Weinert, Phys. Rev. Lett. **50**, 761 (1983).
[35]N.-X. Chen and S. Rabii (unpublished).
[36]Th. Fauster, F. J. Himpsel, J. E. Fischer, and E. W. Plummer, Phys. Rev. Lett. **51**, 430 (1983).
[37]L. Pietronero and S. Strassler, Phys. Rev. Lett. **47**, 593 (1981).
[38]Y. Sato, J. Phys. Soc. Jpn. **24**, 489 (1968).